Corrosion Science 59 (2012) 360–365

Contents lists available at SciVerse ScienceDirect

Corrosion Science

journal homepage: www.elsevier.com/locate/corsci

Short Communication

Improved corrosion resistance and cytocompatibility of magnesium alloy by two-stage cooling in thermal treatment

Ying Zhao [a,b], Guosong Wu [b], Jiang Jiang [b], Hoi Man Wong [a], Kelvin W.K. Yeung [a,*], Paul K. Chu [b,*]

[a] Department of Orthopaedics & Traumatology, The University of Hong Kong, Pokfulam Road, Hong Kong, China
[b] Department of Physics and Materials Science, City University of Hong Kong, Tat Chee Avenue, Kowloon, Hong Kong, China

ARTICLE INFO

Article history:
Received 23 September 2011
Accepted 13 March 2012
Available online 21 March 2012

Keywords:
A. Magnesium
B. EIS
B. Polarization
C. Interfaces

ABSTRACT

A two-stage post-solution cooling procedure including 90 min of furnace cooling and subsequent water quenching is used to modify the morphology and distribution of the β-phase in magnesium–aluminum–zinc alloy. After this special process, the original coarse particle-like β-phase disappears and large-area fine lamellar (α + β) precipitates emerge. Dissolution of the coarse β-phase reduces the galvanic effects and produces the Al-rich α-phase matrix, whereas precipitation of the fine lamellar (α + β) micro-constituent forms a large number of almost continuous β-phase barrier. The microstructural change enhances the bio-corrosion resistance and cytocompatibility of magnesium alloy.

1. Introduction

Magnesium alloys constitute a new class of biomedical implants due to the unique biodegradability in the physiological environment and elastic modulus similar to that of human bone [1–5]. However, different from Ti alloys, CoCr alloys, and stainless steels, direct application of magnesium is not straightforward because the interface between the biomedical implant and tissues is dynamic and uncontrolled and rapid degradation can occur [6]. In particular, human body fluids and blood plasma contain chloride ions that accelerate corrosion of magnesium alloys producing hydrogen gas and localized basification [2]. Consequently, proper control of the degradation process of magnesium alloys is imperative. Much research has been devoted to the identification of effective ways to retard the degradation rate [7–10]. For instance, Zberg et al. [11] proposed the use of Mg–Zn–Ca bulk metal glasses in biomedical implants. Because of the large variety of alloying elements in an amorphous single-phase structure, the corrosion resistance can be enhanced and hydrogen evolution can be reduced as well. However, in many common magnesium alloys, like WE43 and AZ91 or newly developed crystalline magnesium alloys, a multi-phase microstructure is needed in order to satisfy mechanical demands, such as strength and ductility [12,13]. In AZ91 magnesium alloy, the β-$Mg_{17}Al_{12}$ phase plays a crucial role in the corrosion behavior. Generally, the β-phase acts as a galvanic cathode to accelerate corrosion of the α-phase due to its very negative free corrosion potential, but when a continuous β-phase network occurs in the corrosion process, the β-phase is changed to a corrosion barrier to hinder corrosion [14,15]. The morphology, distribution, and volume fraction of the β-phase have also been shown to influence the corrosion resistance [16,17].

Based on the above understanding, one way to improve the corrosion resistance is to minimize the β-phase to avoid the cathodic effect. Zhou et al. [18] used a solid solution to treat the AZ91 magnesium alloy. However, because of the small Al content and some undissolved phases, no evident improvement was observed in simulated body fluids. The other way to improve the corrosion resistance is to form a continuous β-phase network with barrier effects. Liu et al. [19] investigated the effects of the solid solution and an aging process on the degradation of AZ63 magnesium alloy in simulated body fluids and revealed that the corrosion resistance was enhanced with increasing β-phase. In spite of this interesting observation, the relationship among the cytocompatibility, corrosion resistance, and this multi-phase structure is not well understood, although it is generally agreed that enhanced cytocompatibility can be obtained by improving the corrosion resistance [20]. In this paper, we describe an efficient heating and cooling process to modify the β-phase to reduce the degradation rate and enhance the cytocompatibility.

2. Materials and methods

An commercial magnesium alloy AZ91 (91.27 wt.% Mg, 7.76 wt.% Al, 0.79 wt.% Zn, 0.10 wt.% Mn, 0.08 wt.% Si) ingot was

* Corresponding authors. Tel.: +852 22554654; fax: +852 28174392 (K.W.K. Yeung), tel.: +852 34427724; fax: +852 34420542 (P.K. Chu).
E-mail addresses: wkkyeung@hku.hk (K.W.K. Yeung), paul.chu@cityu.edu.hk (P.K. Chu).

0010-938X/$ - see front matter © 2012 Elsevier Ltd. All rights reserved.
http://dx.doi.org/10.1016/j.corsci.2012.03.020

cut into pieces with dimensions of 10 mm × 10 mm × 5 mm before undergoing thermal treatment as shown in Fig. 1. The furnace was first heated from 23 to 410 °C at the rate of 10 °C/min and kept at 410 °C for 24 h. The furnace cooled naturally for 90 min after which the temperature dropped to 213 °C. The samples were then taken out of the furnace and quenched in 10 °C water. Afterwards, the samples were mechanically polished using up to 5 μm diamond paste and ultrasonically washed in pure acetone and ethanol. The microstructure of the samples was evaluated by scanning electron microscopy (SEM, JSM5200) and X-ray diffraction (XRD, Philips X'pert diffractometer) with Cu K_α radiation ($\lambda = 0.154056$ nm) at room temperature.

The electrochemical experiments in simulated body fluids (SBF) [21] and a complete cell culture medium consisting of a mixture of Dulbecco's modified eagle medium (Invitrogen Cat No.11995-040) and 10% fetal calf serum (Hyclone Cat No. SV30087.02) were performed on a Zahner Zennium electrochemical workstation using the three-electrode technique [22]. The potential was referenced to a saturated calomel electrode (SCE) and the counter electrode was a platinum sheet. The samples with a surface area of 10 × 10 mm^2 were exposed to the solution at 37 °C. The EIS measurement was carried out after stabilization in the solution for an hour. The data were recorded from 100 kHz to 100 mHz with a 5 mV sinusoidal perturbing signal at the open-circuit potential. The polarization curves were acquired at a scanning rate of 1 mV/s after immersion for 1 h.

Mouse MC3T3-E1 pre-osteoblasts were used to investigate cell adhesion on the AZ91 alloy surface. Prior to cell cultivation, the samples were sterilized in 75% (v/v) ethanol for 40 min and rinsed three times with sterile phosphate buffered saline (PBS). The MC3T3-E1 pre-osteoblasts were seeded on each sample in 24-well tissue culture plates at a density of 5 × 10^4 cells per well and then cultured for 5 h. Afterwards, the seeded samples were rinsed twice with sterile PBS and fixed with 2% polyoxymethylene. The cytoskeleton protein F-actin was stained with phalloidinfluorescein isothiocyanate (Sigma) and the nuclei were counterstained with Hoechst33342 (sigma). The cell pictures were taken on a fluorescence microscope (Carl Zeiss Axio Observer).

In order to observe proliferation of the MC3T3-E1 pre-osteoblasts on the treated surfaces, 3 × 10^4 cells per well (initial density) were cultured and the medium was renewed every day. After culturing for 1, 3, and 7 days, the samples with the seeded cells were rinsed twice with sterile PBS and transferred to fresh 24-well tissue culture plates. A cell count kit-8 (CCK-8 Beyotime, China) was employed to determine quantitatively the viable cells. The culture medium with 10% CCK-8 was added to these samples. After incubation for 4 h, the solution was aspirated and the absorbance was measured on a Power wave microplate spectrophotometer (BioTek, USA) at a wavelength of 450 nm. The statistical analysis was performed based on the one-way ANOVA analysis and a p value less than 0.05 was considered to be statistically significant.

3. Results and discussion

Fig. 2 shows the XRD spectra of the AZ91 sample before and after the heat treatment. In addition to the primary α-phase, the β-phase ($Mg_{17}Al_{12}$) can be observed from both samples. The volume fraction of the β-phase decreases slightly after the thermal process. Fig. 3a–d illustrates the microstructure evolution. As shown in Fig. 3a and b, the as-received AZ91 alloy contains the primary α-phase, coarse β-phase particles, and fine (α + β) eutectic phase. After the heat treatment, the coarse β-phase disappears and a large-area fine lamellar (α + β) micro-constituent emerges (Fig. 3c and d). When the AZ91 alloy is heated to 410 °C for 24 h, the eutectic phase of the fine (α + β) lamellar arrangement and coarse β particles dissolve in the α-phase matrix leading to an Al-containing super-saturated α-phase matrix [18]. In the subsequent cooling process inside the furnace, the temperature drops slowly from 410 to 213 °C. This induces precipitation of Al atoms from the super-saturated matrix to finally form fine continuous β precipitates in the fine lamellar (α + β) micro-constituent.

Fig. 4 depicts the morphology of the MC3T3-E1 pre-osteoblasts on the AZ91 alloy after culturing for 5 h revealing focal adhesion and cell spreading. Comparing Fig. 4c and d (heat-treated AZ91) to Fig. 4a and b (as-received AZ91), increasingly organized F-actin is observed from the heat-treated AZ91 and the attached cells exhibit more obvious filopodia and flattened membranes. In contrast, most MC3T3-E1 pre-osteoblasts on the as-received AZ91 fail to spread well although they appear to attach to the sample surface. Filopodia and flattened membranes are good evidence of cell adhesion to the materials surface [23,24]. Therefore, superior cell adhesion can be accomplished on the heat-treated AZ91. In addition, the number of MC3T3-E1 pre-osteoblasts on the heat-treated AZ91 after culturing for 5 h is significantly larger than that on the as-received AZ91, indicating that the special thermal process leads to higher initial cell adhesion in the early culturing stage. Fig. 5 shows the cell viability of mouse MC3T3-E1 pre-osteoblasts after culturing for 1, 3, and 7 days. The amount of adherent cells on the heat-treated AZ91 is significantly higher than that on the as-received AZ91 at each time point revealing improved cell viability and cell proliferation. Since high osteoblast proliferation probably leads to a larger mass of bone tissues around the implant, more robust bone-implant bonding is expected *in vivo* [25].

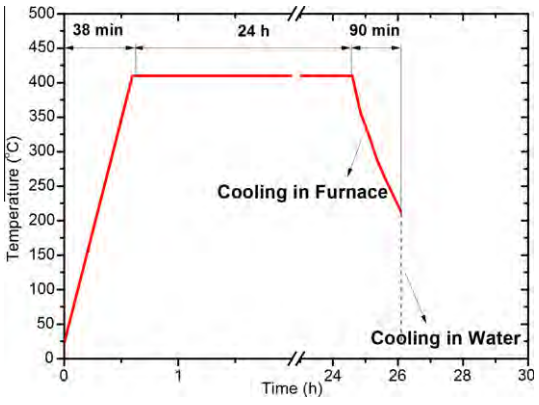

Fig. 1. Schematic diagram of the thermal process.

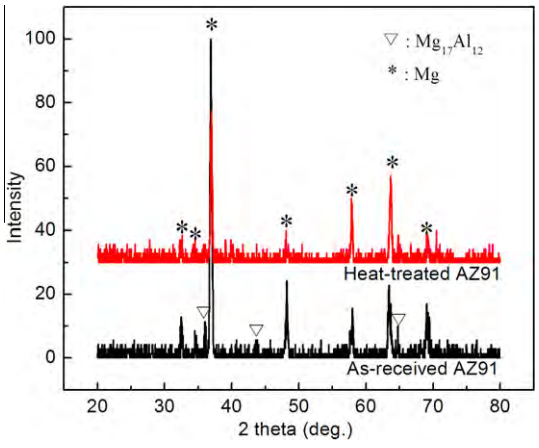

Fig. 2. X-ray diffraction patterns of as-received AZ91 and heat-treated AZ91.

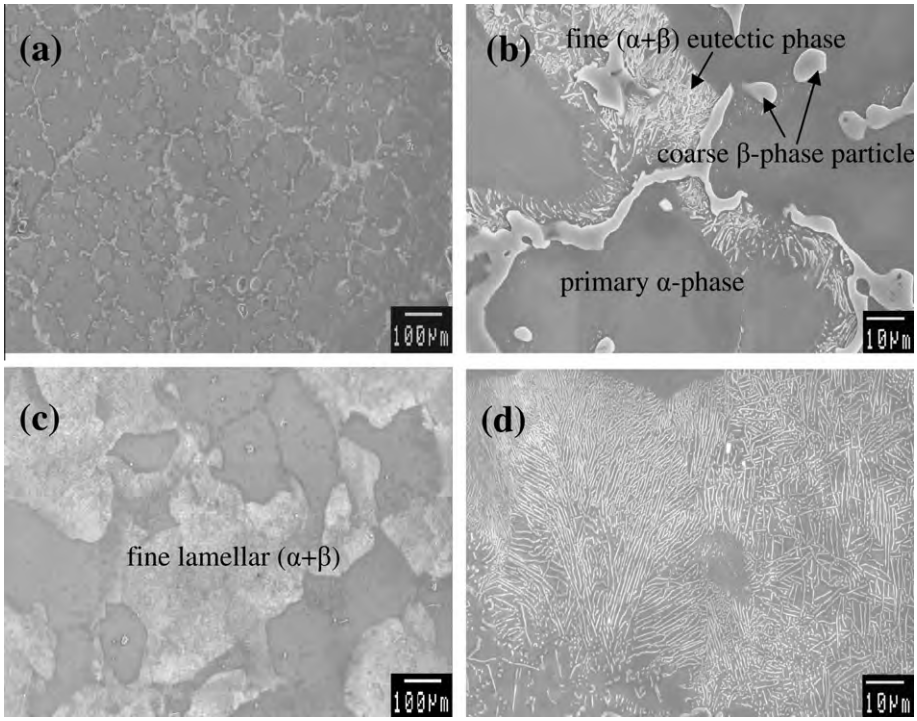

Fig. 3. (a) Microstructure of the as-received AZ91; (b) Magnified β-phase in the as-received AZ91; (c) Microstructure of the heat-treated AZ91; (d) Magnified (α + β) micro-constituent in the heat-treated AZ91.

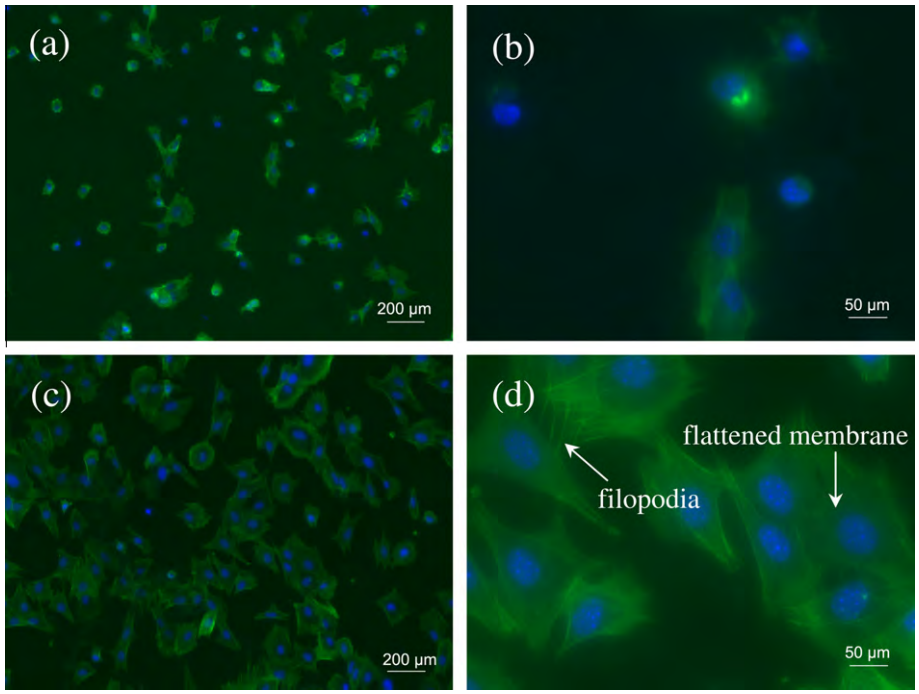

Fig. 4. Fluorescent images of MC3T3-E1 pre-osteoblasts after culturing for 5 h: (a, b) as-received AZ91; (c, d) heat-treated AZ91.

Figs. 6a and 7a display the potentiodynamic polarization curves of the AZ91 alloys acquired in the SBF and cell culture medium, respectively. The polarization curve after the heat treatment shifts to the left. For magnesium alloys, the corrosion current density is usually evaluated by cathodic Tafel extrapolation [26,27]. The regions in cathodic polarization curves reflecting the Tafel features are selected for linear fitting. With regard to the as-received AZ91 and heat-treated AZ91 in SBF, the chosen cathodic regions for fitting are approximately from −1.96 to −1.74 V/SCE and −1.90 to −1.67 V/SCE, respectively. The fitted results are denoted by dotted lines in Fig. 6b and c. The cathodic Tafel slope (b_c) may be obtained from the fitted linear region, as illustrated in Fig. 6b and c. Similarly, the cathodic Tafel slope for the heat-treated AZ91 and as-received AZ91 in the cell culture medium may be

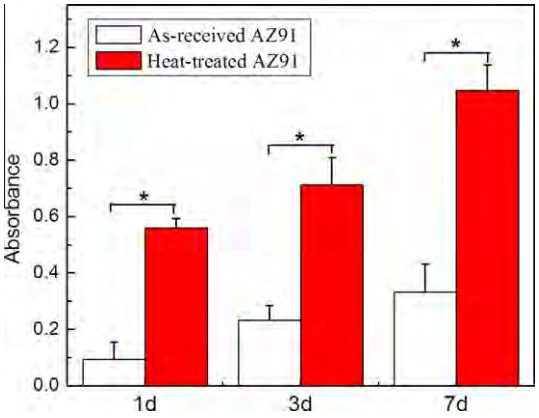

Fig. 5. Cell proliferation assay of MC3T3-E1 pre-osteoblasts cultured on the as-received AZ91 and heat-treated AZ91 for 1, 3 and 7 days. Statistical significant differences between groups are indicated by $^{*}p < 0.05$.

determined as shown in Fig. 7b and c. After the slope is obtained, it can be extrapolated back to the open-circuit corrosion potential (E_{corr}) to obtain the corrosion current density (i_{corr}), as illustrated in Figs. 6a and 7a. The i_{corr}, E_{corr}, and b_c values evaluated from polarization curves are listed in Table 1. Based on the Tafel extrapolation results, the corrosion current density after the heat treatment decreases from 2.0×10^{-4} to 5.4×10^{-5} A/cm^2 in SBF and 1.9×10^{-6} to 7.0×10^{-7} A/cm^2 in the cell culture medium, respectively. Generally, the smaller the corrosion current density, the lower the corrosion rate. Tafel extrapolation is a fast and effective technique to study the corrosion trend and behavior. Different from the hydrogen evolution measurement and weight loss measurement reflecting the whole corrosion process, the corrosion rate determined from Tafel extrapolation is mainly related to the initial surface corrosion [27]. From the perspective of the homogeneity of alloys, the corrosion trend can be estimated by Tafel extrapolation although there may be some differences in the corrosion rate obtained by different methods. Previous studies have confirmed that the corrosion trend estimated by Tafel extrapolation is in accordance with the results of hydrogen evolution and weight loss measurements for heat-treated AZ91D magnesium alloys [18,28]. The above results imply that degradation of AZ91 is indeed retarded after the heat treatment. In addition, the corrosion current density in the cell culture medium is much lower than that in SBF. This may be due to albumin in the cell culture medium forming a corrosion-blocking layer on magnesium [29]. Fig. 6d and e shows the SEM surface micrographs of the as-received AZ91 and heat-treated AZ91 after polarization tests in SBF, respectively. A large number of serious corrosion cracks are shown on the as-received AZ91 surfaces, whereas the heat-treated AZ91 suffers less corrosive attack. The result suggests that dramatic physical and chemical changes occur at the interface between the as-received AZ91 and

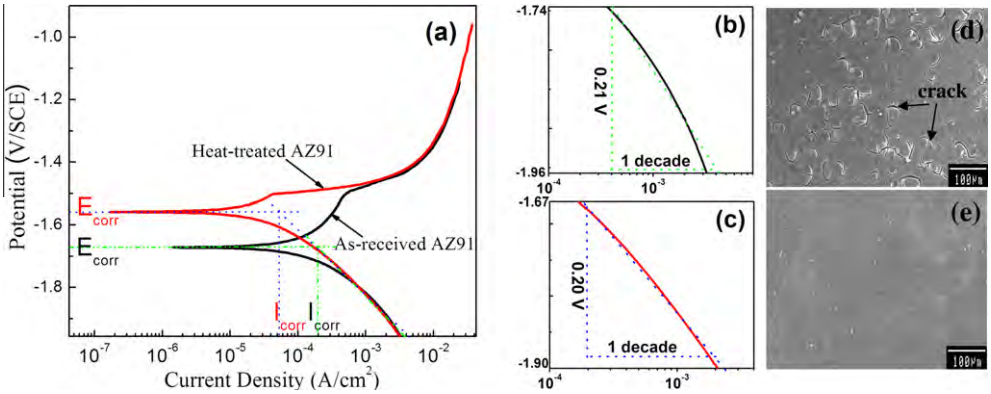

Fig. 6. (a) Polarization curves of as-received AZ91 and heat-treated AZ91 in SBF; cathodic Tafel region of (b) the as-received AZ91 in SBF and (c) the heat-treated AZ91 in SBF, fitting lines denoted by dotted lines; SEM micrographs of (d) as-received AZ91 and (e) heat-treated AZ91 after polarization test in SBF.

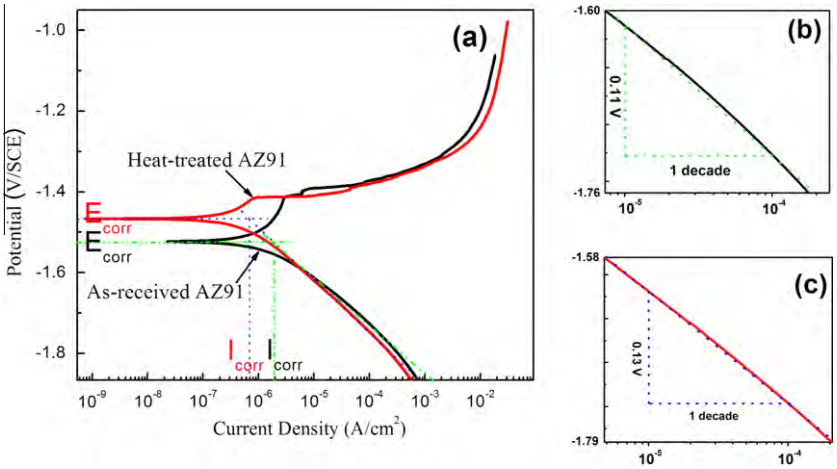

Fig. 7. (a) Polarization curves of as-received AZ91 and heat-treated AZ91 in cell culture medium; cathodic Tafel region of (b) the as-received AZ91 in cell culture medium and (c) the heat-treated AZ91 in cell culture medium, fitting lines denoted by dotted lines.

Table 1
i_{corr}, E_{corr} and b_c values evaluated from polarization curves.

	i_{corr} (A/cm^2)	E_{corr} (V/SCE)	b_c (V/decade)
As-received AZ91 in SBF	2.0×10^{-4}	−1.67	0.21
Heat-treated AZ91 in SBF	5.4×10^{-5}	−1.56	0.20
As-received AZ91 in cell culture medium	1.9×10^{-6}	−1.53	0.11
Heat-treated AZ91 in cell culture medium	7.0×10^{-7}	−1.47	0.13

aggressive media. In comparison, heat treatment creates a more stable interface and it is consistent with the polarization curves.

Regardless of the media, the heat-treated samples show larger capacitive arcs in the EIS spectra than the untreated sample (Fig. 8a and b). Since a larger diameter arc represents better corrosion resistance, the EIS results confirm that the heat treatment can improve the corrosion resistance of the AZ91 magnesium alloys. In order to explain the EIS spectra, an equivalent circuit is proposed to model the alloy/solution system using ZSimpWin 3.20 software and the corresponding fitted data are presented in Fig. 8c. This model can be described as $R_s(R_fCPE_f)(R_tCPE_{dl})$, where R_s represents the solution resistance, R_t is the charge transfer resistance, R_f represents the resistance of the surface film produced in the corrosion process, the constant phase element component CPE_{dl} represents the capacitance of the electric double layer, and CPE_f is the capacitance of the surface film produced in the corrosion process. The

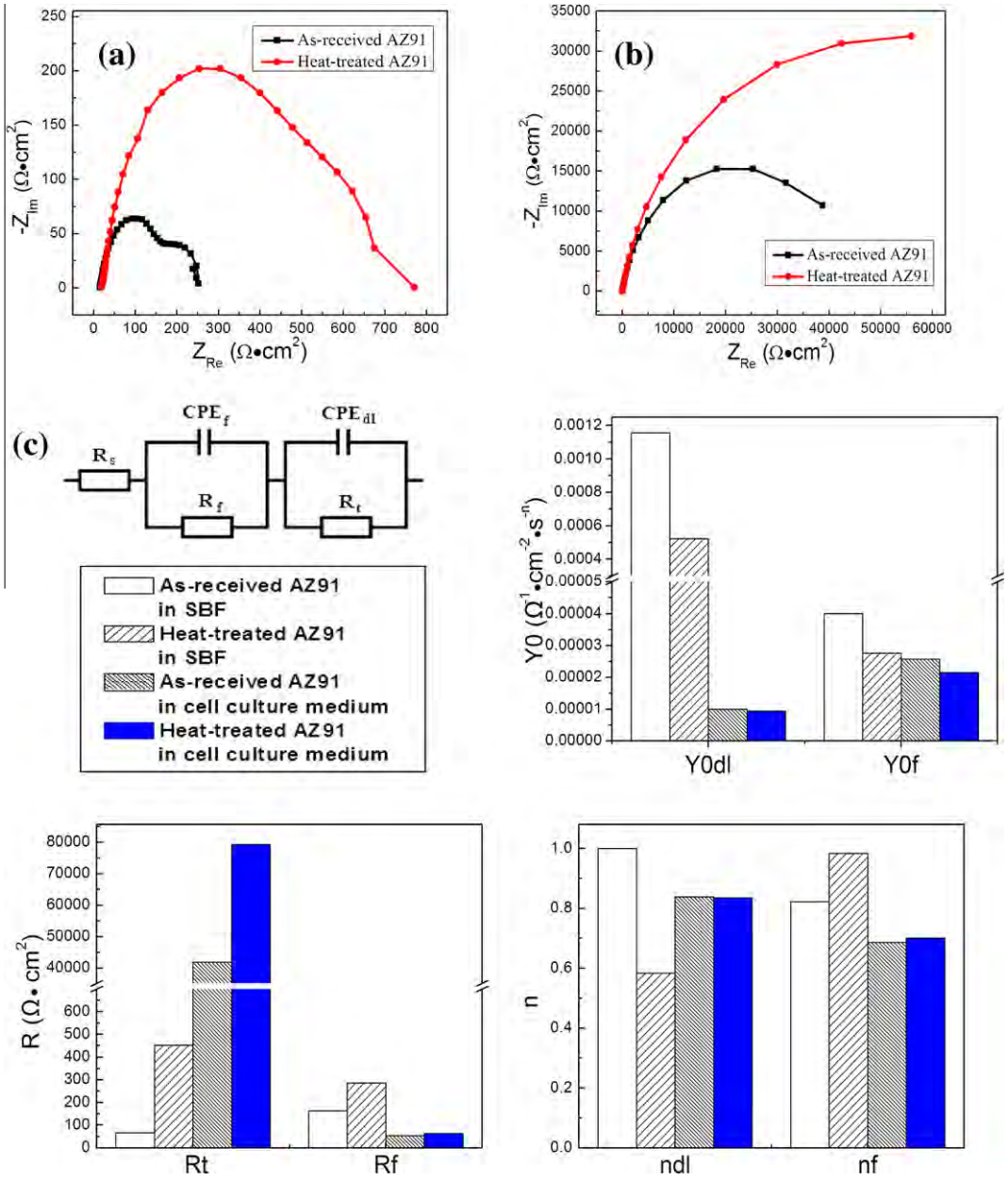

Fig. 8. (a) Nyquist plots acquired in SBF; (b) Nyquist plots acquired in cell culture medium; (c) Equivalent circuit and the fitted results: R_f and R_t, $Y0_f$ and $Y0_{dl}$ and n_f and n_{dl}.

CPE_{dl} (or CPE_f) value is defined by two values, $Y0_{dl}$ (or $Y0_f$) and n_{dl} (or n_f). Here, n_{dl} and n_f are indices of the dispersion effects of CPE_{dl} and CPE_f, respectively, representing deviations from the ideal capacitance due to the inhomogeneity and roughness of the electrode on the micro scale [22]. The value of n always has the following range: $0 < n \leqslant 1$. If n is equal to 1, CPE_{dl} (or CPE_f) is identical to that of a capacitor. The fitted results show that R_t and R_f increase while $Y0_{dl}$ and $Y0_f$ decrease after the thermal process. Larger R_f and R_t reveal the formation of a more compact corrosion product layer on the sample surface and higher resistance to magnesium dissolution, whereas smaller $Y0_{dl}$ and $Y0_f$ correspond to higher values of R_t and R_f, respectively in the experiment, indicating that after the thermal process, there is greater corrosion stability. All the results indicate that the heat treatment improves the corrosion resistance of AZ91 magnesium alloy.

The high degradation rate of magnesium usually results in hydrogen evolution, metal dissolution, and local alkalization. Because cells are very sensitive to environmental fluctuations, any dramatic physical and chemical changes around them can produce deleterious and sometimes fatal effects [2,30–32]. As shown by our results, rapid degradation of magnesium occurring at the interface between the as-received AZ91 and corrosive media adversely affects cell growth. After the special thermal process, the large-area fine lamellar ($\alpha + \beta$) micro-constituent substitutes for the coarse particle-like β-phase to provide a large number of an almost continuous β-phase barrier to retard corrosion. Proper reduction of the degradation rate of magnesium not only creates a relatively stable interface for cell adhesion and growth but also retards the release of corrosion products to reduce the cytotoxicity, therefore finally resulting in the enhanced cytocompatibility.

In the past years, the solution process in conjunction with aging has become an important method to modify the β-phase but it is usually quite time consuming [18]. In comparison, the process reported here is much more efficient. Although homogenization annealing (i.e. several hours heating at a certain temperature plus air-cooling) as an efficient method has been proposed, no evident improvement in the corrosion resistance has been found [16,33]. Therefore, this new thermal technique can expedite the acceptance of Mg by the biomedical industry.

4. Conclusion

Effective two-stage cooling after solution treatment significantly changes the microstructure of magnesium–aluminum–zinc alloy. In this process, the large-area fine lamellar ($\alpha + \beta$) micro-constituent substitutes for the coarse particle-like β-phase, providing a large number of an almost continuous β-phase barrier to retard corrosion. This microstructure evolution improves the bio-corrosion resistance in both SBF and cell culture medium. At the same time, proper reduction of the degradation rate retards the release of corrosion products and creates a relatively stable interface for cell growth, leading to improved cytocompatibility of magnesium–aluminum–zinc alloys.

Acknowledgements

This work was jointly supported by HKU Seed Funding for Basic Research and the Hong Kong Research Grant Council General Research Fund #718507, #123708, and #112510.

References

[1] F. Witte, V. Kaese, H. Haferkamp, E. Switzer, *In vivo* corrosion of four magnesium alloys and the associated bone response, Biomaterials 26 (2005) 3557–3563.
[2] G. Song, Control of biodegradation of biocompatible magnesium alloys, Corros. Sci. 49 (2007) 1696–1701.
[3] N.T. Kirkland, J. Lespagnol, N. Birbilis, M.P. Staiger, A survey of bio-corrosion rates of magnesium alloys, Corros. Sci. 52 (2010) 287–291.
[4] N.I.Z. Abidin, A.D. Atrens, D. Martin, A. Atrens, Corrosion of high purity Mg, Mg2Zn0.2Mn, ZE41 and AZ91 in Hank's solution at 37 °C, Corros. Sci. 53 (2011) 3542–3556.
[5] E. Zhang, L. Xu, K. Yang, Formation by ion plating of Ti-coating on pure Mg for biomedical applications, Scr. Mater. 53 (2005) 523–527.
[6] R. Xu, G. Wu, X. Yang, T. Hu, Q. Lu, P.K. Chu, Controllable degradation of biomedical magnesium by chromium and oxygen dual ion implantation, Mater. Lett. 65 (2011) 2171–2173.
[7] H.M. Wong, W.K. Yeung, P.K. Chu, D.K. Luk, M.C. Cheung, A biodegradable polymer-based coating to control the performance of magnesium alloy orthopaedic implants, Biomaterials 31 (2010) 2084–2096.
[8] R. Arrabal, E. Matykina, F. Viejo, P. Skeldon, G.E. Thompson, Corrosion resistance of WE43 and AZ91D magnesium alloys with phosphate PEO coatings, Corros. Sci. 50 (2008) 1744–1752.
[9] A. Bakkar, V. Neubert, Improving corrosion resistance of magnesium-based alloys by surface modification with hydrogen by electrochemical ion reduction (EIR) and by plasma immersion ion implantation (PIII), Corros. Sci. 47 (2005) 1211–1225.
[10] Y. Zhao, G. Wu, H. Pan, K.W.K. Yeung, P.K. Chu, Formation and electrochemical behavior of Al and O plasma-implanted biodegradable Mg–Y–RE alloy, Mater. Chem. Phys. 132 (2012) 187–191.
[11] B. Zberg, P.J. Uggowitzer, J.F. Löffler, MgZnCa glasses without clinically observable hydrogen evolution for biodegradable implants, Nat. Mater. 8 (2009) 887–891.
[12] G. Yuan, Y. Sun, W. Ding, Effects of Sb addition on the microstructure and mechanical properties of az91 magnesium alloy, Scr. Mater. 43 (2000) 1009–1013.
[13] X.N. Gu, W.R. Zhou, Y.F. Zheng, Y. Cheng, S.C. Wei, S.P. Zhong, T.F. Xi, L.J. Chen, Corrosion fatigue behaviors of two biomedical Mg alloys – AZ91D and WE43 – in simulated body fluid, Acta Biomater. 6 (2010) 4605–4613.
[14] G. Ballerini, U. Bardi, R. Bignucolo, G. Ceraolo, About some corrosion mechanisms of AZ91D magnesium alloy, Corros. Sci. 47 (2005) 2173–2184.
[15] G. Song, A. Atrens, Understanding magnesium corrosion – a framework for improved alloy performance, Adv. Eng. Mater. 5 (2003) 837–858.
[16] M.C. Zhao, M. Liu, G. Song, A. Atrens, Influence of the β-phase morphology on the corrosion of the Mg alloy AZ91, Corros. Sci. 50 (2008) 1939–1953.
[17] T. Zhang, Y. Li, F. Wang, Roles of β phase in the corrosion process of AZ91D magnesium alloy, Corros. Sci. 48 (2006) 1249–1264.
[18] W. Zhou, T. Shen, N.N. Aung, Effect of heat treatment on corrosion behaviour of magnesium alloy AZ91D in simulated body fluid, Corros. Sci. 52 (2010) 1035–1041.
[19] C. Liu, Y. Xin, G. Tang, P.K. Chu, Influence of heat treatment on degradation behavior of bio-degradable die-cast AZ63 magnesium alloy in simulated body fluid, Mater. Sci. Eng., A 456 (2007) 350–357.
[20] J. Li, Y. Song, S. Zhang, C. Zhao, F. Zhang, X. Zhang, T. Tang, In vitro responses of human bone marrow stromal cells to a fluoridated hydroxyapatite coated biodegradable Mg–Zn alloy, Biomaterials 31 (2010) 5782–5788.
[21] T. Kokubo, H. Kushitani, S. Sakka, T. Kitsugi, T. Yamamuro, Solutions able to reproduce *in vivo* surface-structure changes in bioactive glass-ceramic A–W, J. Biomed. Mater. Res. 24 (1990) 721–734.
[22] Y.C. Xin, T. Hu, P.K. Chu, Degradation behavior of pure magnesium in simulated body fluids with different concentrations of HCO_3^-, Corros. Sci. 53 (2011) 1522–1528.
[23] G. Orsini, B. Assenza, A. Scarano, M. Piatelli, A. Piattelli, Surface analysis of machined versus sandblasted and acid-etched titanium implants, Int. J. Oral. Maxillofac. Implants 15 (2000) 779–784.
[24] H.H. Huang, S.J. Pan, Y.L. Lai, T.H. Lee, C.C. Chen, F.H. Lu, Osteoblast-like cell initial adhesion onto a network-structured titanium oxide layer, Scr. Mater. 51 (2004) 1017–1021.
[25] L. Zhao, S. Mei, P.K. Chu, Y. Zhang, Z. Wu, The influence of hierarchical hybrid micro/nano-textured titanium surface with titania nanotubes on osteoblast functions, Biomaterials 31 (2010) 5072–5082.
[26] Z.M. Shi, M. Liu, A. Atrens, Measurement of the corrosion rate of magnesium alloys using Tafel extrapolation, Corros. Sci. 52 (2010) 579–588.
[27] M.C. Zhao, M. Liu, G.L. Song, A. Atrens, Influence of pH and chloride ion concentration on the corrosion of Mg alloy ZE41, Corros. Sci. 50 (2008) 3168–3178.
[28] G.L. Song, A.L. Bowles, D.H. St John, Corrosion resistance of aged die cast magnesium alloy AZ91D, Mater. Sci. Eng., A 366 (2004) 74–86.
[29] C.L. Liu, Y.C. Xin, X.B. Tian, P.K. Chu, Degradation susceptibility of surgical magnesium alloy in artificial biological fluid containing albumin, J. Mater. Res. 22 (2007) 1806–1814.
[30] F. Witte, N. Hort, C. Vogt, S. Cohen, K.U. Kainer, R. Willumeit, F. Feyerabend, Degradable biomaterials based on magnesium corrosion, Curr. Opin. Solid State Mater. Sci. 12 (2008) 63–72.
[31] Y.C. Xin, J. Jiang, K.F. Huo, G.Y. Tang, X.B. Tian, P.K. Chu, Corrosion resistance and cytocompatibility of biodegradable surgical magnesium alloy coated with hydrogenated amorphous silicon, J. Biomed. Mater. Res. A 89A (2009) 717–726.
[32] K.C. Popat, L. Leoni, C.A. Grimes, T.A. Desai, Influence of engineered titania nanotubular surfaces on bone cells, Biomaterials 28 (2007) 3188–3197.
[33] Y. Wang, G. Liu, Z. Fan, Microstructural evolution of rheo-diecast AZ91D magnesium alloy during heat treatment, Acta Mater. 54 (2006) 689–699.